the order of a wavelength, then we find

$$|\alpha_2|^2/|\alpha_1|^2 \simeq \frac{v'}{v_{Gy}} \frac{u}{\omega \partial v/\partial \omega}\Big|_{\omega=\Omega_0}, \quad (5.17)$$

where we have neglected higher-order terms in $u/(\omega \partial v/\partial \omega)$. Here v' is a characteristic velocity defined as

$$v' = \Omega_0 \delta.$$

When $|\alpha_2|$ is small compared to $|\alpha_1|$, the energy density in the surface wave is

$$\bar{w} \simeq -\tfrac{1}{4}\omega^2 \partial v/\partial \omega \xi^\dagger \xi|_{\omega=\Omega_0}, \quad (5.18)$$

which shows that

$$\Delta\omega \simeq -jS_y/2W. \quad (5.19)$$

Numerical calculations given by Lim[17] have shown that the leaky waves very often have an attenuation per period which is only $10^{-4}-10^{-3}$. In these cases the approximate results given above should be quite good.

ACKNOWLEDGMENT

The authors acknowledge the financial support received from the Norwegian Council of Scientific Research.

PHYSICAL REVIEW VOLUME 184, NUMBER 3 15 AUGUST 1969

Low-Temperature Thermal Conductivity of Impure Insulators

PAUL ERDÖS* AND STEPHEN B. HALEY
Department of Physics, The Florida State University, Tallahassee, Florida 32306
(Received 17 February, 1969)

The low-temperature thermal transport properties of an insulating crystal with an arbitrary concentration of randomly located phonon scattering centers are found for slab geometry. The phonon distribution function, the distribution of temperature, the Kapitza resistance at the boundaries, and the heat flux are evaluated by analytically and numerically solving the complete Boltzmann equation with energy-dependent scattering cross section.

I. INTRODUCTION

THE problem of heat conduction through an electrically insulating crystal at low temperatures leads to the formulation of the Boltzmann transport equation for phonons. In this equation, the collision operator plays the most significant part because it is responsible for thermal resistance. The collision operator introduces into the equation the effect of the two most important scattering mechanisms: scattering of phonons by stationary obstacles (impurities, defects, boundaries, etc.) and scattering of phonons by phonons. Because of mathematical difficulties it has been an accepted practice not to solve the Boltzmann transport equation as it is, but to treat it with the aid of the *relaxation-time approximation.*

A large body of experimental observations has been successfully explained in terms of this approximation, relying, in particular, on the work of Callaway.[1] At the same time, however, a large number of questions remain unanswered. They motivate the present work.

The first question we raise, concerns the validity of the relaxation-time approximation: If, by suitable choice of the available parameters, the theoretical curves resulting from the relaxation-time approximation may be fitted to the experimental data, does this mean that further conclusions of the theory are correct? This question cannot be answered without working out the more exact theory, since the relaxation-time approximation is not capable of estimating its own accuracy.

As we shall see in the discussion (see, in particular, Sec. VIII the discussion of Fig. 8), some conclusions of the approximate theory are born out; others are contradicted by the results of a more exact theory. Questioning further, let us point out that there are some basic difficulties with the relaxation-time approximation.

According to this approximation, if more than one relaxation (scattering) mechanism is present, the system should approach equilibrium faster, than if any one of the individual mechanisms alone is active: More channels enable quicker relaxation. The speed of relaxation being measured by the inverse relaxation time, this means

$$\frac{1}{\tau} > \max_i\left(\frac{1}{\tau_i}\right), \quad (1.1)$$

where τ is the combined relaxation time, and the τ_i are the individual relaxation times. We contend that in order for the concept of relaxation times to make physical sense, this equation must be valid.

It has been customary to assume additivity of n

* On leave from the International Business Machines Corporation, Zürich Research Laboratory, Switzerland.

[1] J. Callaway, Phys. Rev. 113, 1046 (1959).

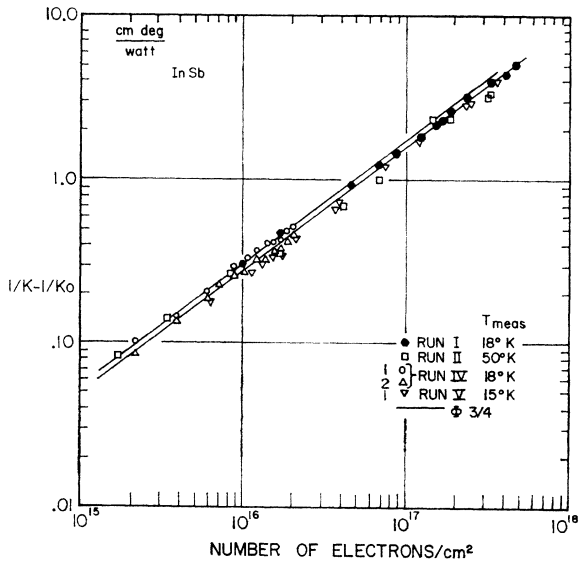

FIG. 1. The reciprocal $1/\kappa$ of the thermal conductivity of InSb containing point defects less the reciprocal $1/\kappa_0$ of the conductivity of the sample without defects. The defects are created by electron irradiation, hence the scale of the abscissa is proportional to the defect concentration. [After F. L. Vook, Phys. Rev. **149**, 631 (1966).]

reciprocal relaxation times, i.e., to set

$$\frac{1}{\tau}=\sum_{i=1}^{n}\frac{1}{\tau_i}. \tag{1.2}$$

It was realized earlier (see Ref. 1) that (1.2) is not exactly valid. However, recent provocative results show, that even (1.1) is invalid. Hence, under quite natural conditions, the concept of relaxation times loses its meaning.

The results referred to have been obtained from a computer experiment by Payton, Rich, and Visscher.[2] Their results show, that in a plane lattice with defect scattering, the introduction of anharmonicity (i.e., phonon-phonon scattering) increases the thermal conductivity instead of reducing it. In terms of relaxation times this means

$$\frac{1}{\tau}<\frac{1}{\tau_{\text{imp}}}, \text{ and } \frac{1}{\tau}<\frac{1}{\tau_{\text{ph-ph}}}. \tag{1.3}$$

Qualitatively, this may be understood,[3] but a transport theory based on the concept of relaxation times cannot account for these observations.

It is only fair to point out, however, that in the limit of weak impurity scattering, our result (5.10) agrees with the one obtained by Callaway,[1] who combines the inverse relaxation times of impurity and boundary scattering. In this limit, then, the relaxation-time approximation is good.

Objectives and Organization

In this paper, we treat thermal conductivity at low temperatures, at which the phonon-phonon scattering is negligible, hence the question of the additivity of relaxation times will not be dealt with. However, as a first step in the direction towards a complete solution of the transport equation, we shall treat impurity scattering using the full collision operator, and hence show how to completely avoid the relaxation-time approximation. This exact theory not only allows us to calculate the macroscopic thermal conductivity, but gives us the phonon distribution function inside the sample. Hence we will obtain a clear picture of the nonequilibrium situation which prevails during thermal conduction, and will be able to answer a long-standing question: What is the temperature distribution inside the sample?

Finally, we shall compare our results with experimental observations. The most striking features of these may be pointed out in Fig. 1, reproduced from Vook.[4] In the range of defect concentration and temperatures used by Vook in InSb,

(1) the thermal resistivity is proportional to the $\frac{3}{4}$ power of the number of scattering centers.
(2) The thermal resistivity is—within the limits of experimental error—independent of the temperature.

In the following, an analysis is carried through, which correctly reproduces these experimental results. This analysis is based on what we believe is the first complete solution of the Boltzmann integro-differential equation for phonons using an energy-dependent scattering cross section. The foundations to this work are laid in an earlier publication.[5] In the present paper, we go considerably further in two directions.

First, we develop an approximate analytical solution, which is better[6] than the one in Ref. 5. In particular, it gives the spatial dependence of the distribution function. Second, we develop a numerical solution, which may be made as accurate as the purpose requires. This development was indispensable, because the analytical solutions are only valid in the cases where the phonon mean free path is either much larger or much smaller than the dimensions of the sample. The numerical solution, developed for the intermediate region, is also valid for the two limits of large and small mean free path, and of course coincides with the analytical solution in these regions.

[2] D. N. Payton, III, M. Rich, and W. M. Visscher, Phys. Rev. **160**, 706 (1967).
[3] J. A. Krumhansl and P. S. Pershan, discussion remarks at the Gordon Research Conference on Disordered Structures, Meriden, N. H., 1968 (unpublished).
[4] F. L. Vook, Phys. Rev. **149**, 631 (1966).
[5] P. Erdös, Phys. Rev. **138**, A1200 (1965).
[6] We are indebted to Professor J. Tavernier of the University of Paris for his stimulating communication on this subject. See also J. Tavernier, J. Phys. (Paris) **28**, Suppl. 2, C1 (1967).

We formulate the transport equation for the phonon distribution function in a slab with point scattering of the phonons. This equation is then reduced to an equation for the *change* of the distribution function due to the scattering, the function in the absence of scattering being known.

We introduce the parameter *free-path ratio* Λ, defined as

$$\Lambda=\lambda/2a, \tag{1.4}$$

where λ is the free path of those phonons which have the largest contribution per unit energy range to the heat flux in the presence of scattering (see Appendix A), and 2a is the slab thickness.

The asymptotic solutions are found next, and the two observables—temperature and heat flux—calculated in the limits of $\Lambda\gg1$ and $\Lambda\ll1$. The numerical solution follows, along with the final results for the distribution function, temperature, and heat flux for certain representative values of five parameters. These five parameters are the sound velocity c_s, the slab center temperature T_m, the temperature difference ΔT between the reservoirs, the free-path ratio Λ, and, finally, the slab thickness $2a$.

II. BOUNDARY CONDITIONS

Realistic boundary conditions for the distribution function of phonons transporting energy across a medium bounded by two infinite planes acting as thermal reservoirs at temperatures T_1 and T_2 have been formulated in Ref. 5. For convenience, we recapitulate some of the definitions of Ref. 5. The reservoirs act as perfect black bodies, emitting phonons into the slab according to Planck's law and absorbing all incident phonons. The mean temperature of the slab is

$$T_m=\tfrac{1}{2}(T_1+T_2)=T_1-\tfrac{1}{2}\Delta T, \tag{2.1}$$

where

$$\Delta T=T_1-T_2 \tag{2.2}$$

is the temperature difference between the reservoirs. In the absence of scattering centers, the distribution function for phonons at any point in the slab is given by

$$f^0=\theta(\mu)f^0(T_1)+\theta(-\mu)f^0(T_2), \tag{2.3}$$

where

$$f^0(T_m)=(e^{\epsilon_k/k_BT_m}-1)^{-1}, \tag{2.4}$$

$\epsilon_k=c_s\hbar k$ is the phonon energy, $\mathbf{k}$ is the phonon wave vector, c_s is the sound velocity, μ is the cosine of the angle α between $\mathbf{k}$ and the x axis, which is perpendicular to the plane boundaries, and θ is defined by

$$\begin{aligned}\theta(\mu)&=1 \quad \text{for} \quad 0<\mu\leq1,\\ &=0 \quad \text{for} \quad -1\leq\mu<0.\end{aligned} \tag{2.5}$$

III. IMPURITY SCATTERING

In the presence of impurities, the phonon distribution function for one polarization branch becomes

$$f(k,x,\mu)=f^0+f^1(k,x,\mu). \tag{3.1}$$

The first term in (3.1) is the distribution function (2.3) in the absence of impurity-scattering centers, and the last term represents the change of the distribution function due to the scattering by impurities. The distribution function is independent of the azimuthal angle because of the symmetry around the x axis.

In accordance with the assumption made in Sec. II about the interfaces between the reservoirs and the slab, f satisfies the boundary conditions

$$\begin{aligned}f(-a)&=f^0(T_1) \quad \text{for} \quad 0<\mu\leq1,\\ f(a)&=f^0(T_2) \quad \text{for} \quad -1\leq\mu<0,\end{aligned} \tag{3.2}$$

where $2a$ is the distance between the reservoirs, and the origin of the coordinates is midway between them.

We solve the Boltzmann transport equation (see Ref. 5) for phonons:

$$-c_s\mu[\partial f_{\mathbf{k}}(x)/\partial x]=L_{\mathbf{k}}^{\text{imp}}\{f_{\mathbf{k}}(x)\}. \tag{3.3}$$

The collision operator $L_{\mathbf{k}}^{\text{imp}}\{f\}$, due to impurity scattering is given by

$$L_{\mathbf{k}}^{\text{imp}}\{f_{\mathbf{k}}(x)\}=NV\sum_{\mathbf{k}'}[f_{\mathbf{k}}(x)-f_{\mathbf{k}'}(x)]dW_{\mathbf{k}\mathbf{k}'}, \tag{3.4}$$

where N is the number of scattering centers per unit volume, V is the volume of the sample, and $dW_{\mathbf{k}\mathbf{k}'}$ is the transition probability for isotropic, elastic, energy-dependent, impurity scattering given by

$$dW_{\mathbf{k}\mathbf{k}'}=\frac{2\pi}{c_s\hbar^2}\frac{\sigma}{V^2}k^{m-2}\delta(k-k'). \tag{3.5}$$

Rayleigh point scattering, which is characterized by $m=4$, will be used in the numerical calculations. The transition probability is developed in Appendix A, and the scattering strength σ is related to the total scattering cross section and Λ.

Since f^0 does not depend on x, (3.3) becomes

$$-c_s\mu(\partial f^1/\partial x)=L_{\mathbf{k}}^{\text{imp}}\{f^0\}+L_{\mathbf{k}}^{\text{imp}}\{f^1\}. \tag{3.6}$$

Using (2.3) and (3.5), the first collision term is

$$\begin{aligned}L_{\mathbf{k}}^{\text{imp}}\{f^0\}=(N\sigma k^m/2\pi c_s\hbar^2)\{&f^0(T_1)[2\theta(\mu)-1]\\ &+f^0(T_2)[2\theta(-\mu)-1]\},\end{aligned} \tag{3.7}$$

which can be recast in the form

$$L_{\mathbf{k}}^{\text{imp}}\{f^0\}=(N\sigma k^m/2\pi c_s\hbar^2)[f^0(T_1)-f^0(T_2)]S(\mu), \tag{3.8}$$

by defining

$$\begin{aligned}S(\mu)&=1 \quad \text{for} \quad 0<\mu\leq1,\\ &=-1 \quad \text{for} \quad -1\leq\mu<0.\end{aligned} \tag{3.9}$$

The second collision term is

$$L_k^{\text{imp}}\{f^1\}=\frac{N\sigma k^m}{\pi c_s\hbar^2}\left[f^1(k,x,\mu)-\frac{1}{2}\int_{-1}^{1}f^1(k,x,\mu')d\mu'\right]. \quad (3.10)$$

Substituting (3.8) and (3.10) into (3.6), the equation for the change in the phonon distribution function becomes

$$\mu\frac{\partial f^1}{\partial x}+\frac{N\sigma k^m}{\pi c_s^2\hbar^2}f^1=\frac{N\sigma k^m}{2\pi c_s^2\hbar^2}\times\left\{\int_{-1}^{1}f^1(\mu')d\mu'-[f^0(T_1)-f^0(T_2)]S(\mu)\right\}. \quad (3.11)$$

In view of (3.2) and (3.1) this solution must satisfy the boundary conditions

$$\begin{aligned} f^1(k,-a,\mu)&=0 \quad \text{for} \quad 0<\mu\leq 1,\\ f^1(k,a,\mu)&=0 \quad \text{for} \quad -1\leq\mu<0. \end{aligned} \quad (3.12)$$

For convenience throughout the rest of the paper, we set

$$\xi=aN\sigma/\pi c_s^2\hbar^2 \quad \text{and} \quad C^0=f^0(T_1)-f^0(T_2). \quad (3.13)$$

Using the definition of $\Lambda(k)$ from Appendix A, it follows

$$\xi k^m=1/2\Lambda(k). \quad (3.14)$$

Thus, (3.11) becomes

$$4a\Lambda(k)\mu\frac{\partial f^1}{\partial x}+2f^1=\int_{-1}^{1}f^1(\mu')d\mu'-C^0S(\mu). \quad (3.15)$$

If we define f_1^+ and f_1^- by

$$\begin{aligned} f_1^+(k,x,\mu)&\equiv f^1(k,x,\mu) \quad \text{for} \quad 0<\mu\leq 1,\\ f_1^-(k,x,\tilde{\mu})&\equiv f^1(k,x,\mu) \quad \text{for} \quad -1\leq\mu<0, \end{aligned} \quad (3.16)$$

where

$$\tilde{\mu}=-\mu,$$

we see that (3.15) is a set of two coupled integro-differential equations for the functions f_1^+ representing the contribution due to forward scattering and f_1^- that due to back scattering. We rewrite (3.15) as two equations:

$$\begin{aligned} &4a\Lambda(k)\mu\frac{\partial f_1^+}{\partial x}+2f_1^+-\int_0^1 f_1^+(\mu')d\mu'\\ &\qquad-\int_0^1 f_1^-(\mu')d\mu'=-C^0 \quad \text{for} \quad \mu>0 \end{aligned}$$

and (3.17)

$$\begin{aligned} &-4a\Lambda(k)\tilde{\mu}\frac{\partial f_1^-}{\partial x}+2f_1^--\int_0^1 f_1^-(\mu')d\mu'\\ &\qquad-\int_0^1 f_1^+(\mu')d\mu'=C^0 \quad \text{for} \quad \tilde{\mu}>0. \end{aligned}$$

IV. ANALYTIC SOLUTIONS FOR HIGH- AND LOW-IMPURITY-CONCENTRATION LIMITS

Since the phonons are isotropically scattered from random point impurities, we expect that the change f^1 in the phonon distribution function will become almost independent of the angle of propagation of the phonons in the limit of high-impurity concentration. Therefore, in seeking solutions to (3.17) we set $g_0^{\pm}=f_1^{\pm}$ and assume that $g_0^{\pm}$ is weakly dependent on μ (or $\tilde{\mu}$).

According to the mean-value theorem, we have

$$\int_0^1 g_0^-(\mu')d\mu'=g_0^-(\mu_0), \quad (4.1)$$

where μ_0 is a fixed value, $0<\mu_0\leq 1$. Since we assume that g_0^- depends only weakly on μ, we may set

$$g_0^-(\mu_0)=g_0^-(\mu)+r(\mu), \quad (4.2)$$

where μ is now a variable, $0<\mu\leq 1$, and neglect the remainder $r(\mu)$. A similar approximation is made for g_0^+. Since both $\tilde{\mu}$ and μ are positive, we use the single independent variable μ to denote both of them in this section.

This reduces the coupled integro-differential equations to a coupled set of two ordinary inhomogeneous differential equations with μ as a parameter. These are

$$\begin{aligned} &4a\Lambda(k)\mu(dg_0^+/dx)+g_0^+-g_0^-=-C^0 \quad \text{for} \quad \mu>0\\ &\text{and}\\ &-g_0^+-4a\Lambda(k)\mu(dg_0^-/dx)+g_0^-=C^0 \quad \text{for} \quad \mu>0. \end{aligned} \quad (4.3)$$

Adding these equations gives

$$\frac{dg_0^+}{dx}=\frac{dg_0^-}{dx}. \quad (4.4)$$

Using (4.4) and the boundary conditions (3.12), the solutions to (4.3) are

$$\begin{aligned} g_0^+&=-\frac{1}{2a}\frac{[f^0(T_1)-f^0(T_2)]}{1+\mu/\xi k^m}(x+a) \quad \text{for} \quad \mu>0\\ &\text{and}\\ g_0^-&=-\frac{1}{2a}\frac{[f^0(T_1)-f^0(T_2)]}{1-\mu/\xi k^m}(x-a) \quad \text{for} \quad \mu<0. \end{aligned} \quad (4.5)$$

Recalling that these are approximate solutions, we substitute them into Eq. (3.17) and find that some of the terms of order C^0 cancel, leaving a remainder

$$R=\frac{x}{a}C^0\left[\frac{1}{1+\mu/\xi k^m}-\xi k^m\ln(1+1/\xi k^m)\right]. \quad (4.6)$$

We define the *high-impurity-scattering limit* by

$$1/2\Lambda(k_1)\mu=\xi k_1^m/\mu\gg 1 \quad (4.7)$$

with k_1 being the phonon wave number around which the phonon distribution is peaked. In this limit, expansion in powers of $(\xi k_1{}^m)^{-1}$ shows that all terms of order C^0 cancel, leaving

$$R\cong(x/a)C^0[(\tfrac{1}{2}-\mu)/\xi k_1{}^m+0(1/\xi^2 k_1{}^{2m})]\ll C^0. \quad (4.8)$$

Hence the solution is particularly accurate around $\mu=\frac{1}{2}$. The *limit* of *low impurity scattering* is defined by

$$1/2\Lambda(k_1)\mu=\xi k_1{}^m/\mu\ll 1. \quad (4.9)$$

Expansion in powers of $\xi k_1{}^m$ gives

$$R\cong(x/a)C^0\xi k_1{}^m[1/\mu+\ln\xi k_1{}^m+O(\xi k_1{}^m)]\ll C^0. \quad (4.10)$$

Thus, in seeking a solution which is independent of μ for the high-impurity-scattering limit, we have found one which is dependent on μ and which is valid under certain restrictions on μ for both the high- and the low-impurity limits. This is not surprising, because when μ approaches zero the phonons travel almost parallel to the boundaries. For these phonons the probability of encountering an impurity before reaching the other boundary is very high; hence they must be treated as phonons in the high-impurity limit.

To obtain a solution for the middle-impurity-concentration region, we start with the solution found for the low-impurity limit, and apply an iterative process by setting

$$f_1{}^{\pm}=g_0{}^{\pm}+g_1{}^{\pm}. \quad (4.11)$$

Here, g_0 is given by (4.5) and $g_1{}^{\pm}$ is assumed to be almost independent of μ. Substitution of (4.11) into the Boltzmann equations (3.17) again gives a coupled set of ordinary inhomogeneous differential equations

$$4a\Lambda(k)\mu\frac{dg_1{}^+}{dx}+g_1{}^+-g_1{}^-=R \quad \text{for} \quad \mu>0$$

and (4.12)

$$-4a\Lambda(k)\mu\frac{dg_1{}^-}{dx}-g_1{}^++g_1{}^-=R \quad \text{for} \quad \mu>0,$$

with R defined by Eq. (4.6).

The solutions to this set are found in the same manner as g_0 was found. We have

$$g_1{}^{\pm}=-\frac{1}{4}\frac{[f^0(T_1)-f^0(T_2)]}{\gamma^3(1+\gamma)}[\gamma-\mu(1+\gamma)\ln(1+\gamma/\mu)]$$
$$\times\left[\frac{1}{3}\left(\frac{x}{a}\right)^3\mp\gamma\left(\frac{x}{a}\right)^2-\frac{1}{3}\left(\frac{1+3\gamma}{1+\gamma}\right)\left(\frac{x}{a}\mp\gamma\right)\right], \quad (4.13)$$

where

$$\gamma=2\mu\Lambda(k).$$

In the low-impurity-scattering limit, i.e., $\gamma\gg 1$, the function g_0 goes to zero almost as γ^{-2}; however, for $\gamma\ll 1$, the function g_1 grows without bound.

To test the validity of the approximate analytic expression (4.13) for g_1, it was compared with the numerical solution (to be discussed later). The comparison shows that this form of g_1 is very precise in the low-impurity region. The singular dependence of g_1 on μ proscribes any further iteration.

V. MOMENTUM AND ENERGY IN HIGH- AND LOW-IMPURITY-SCATTERING LIMITS CALCULATED FROM THE ANALYTIC SOLUTION g_0

Momentum Density and Heat Flux

The total phonon *momentum density* at any point x in the slab is given by the sum of a contribution P_0 due only to the temperature difference across the pure slab and a negative contribution P_1 due to scattering by the impurity centers. Because of the linear dispersion relation $\epsilon_k=c_s\hbar k$, the total momentum density P is simply related to the total *heat flux* Q and to the thermal conductivity κ by

$$Q=c_s{}^2P=\kappa(\Delta T/2a). \quad (5.1)$$

The total momentum density is

$$P=P_0+P_1=\Omega\int\hbar\mathbf{k}\cdot\hat{x}f_{\mathbf{k}}(x)d^3k, \quad (5.2)$$

where $\hat{x}$ is a unit vector in the x direction, and $\Omega=(2\pi)^{-3}$. As is well known, Eq. (5.2) defines the *quasimomentum* of the phonons; however, for short, P will be called the *momentum* in the sequel. The contribution obtained from f^0 is

$$P_0=2\pi\Omega\hbar\int_0^1\mu d\mu\int_0^\infty k^3C^0dk, \quad (5.3)$$

and that obtained from the analytic solution g_0 in (4.5) is

$$P_1=\Omega\int\hbar k\mu g_0d^3k=-2\pi\Omega\hbar\int_0^1\mu d\mu\int_0^\infty k^3\frac{C^0\xi k^m}{\xi k^m+\mu}dk. \quad (5.4)$$

For the high-impurity-scattering limit we substitute (5.3) and (5.4) into (5.2) to give a combined form

$$P=2\pi\Omega\hbar\int_0^1\mu^2d\mu\int_0^\infty\frac{k^3C^0}{\xi k^m+\mu}dk. \quad (5.5)$$

Note that the momentum density is constant across the slab, as expected for elastic scattering. The integral in k space is evaluated in Appendix B, using the saddle-point method of Laplace. The result is

$$P=\frac{2\pi(m-2)}{2m+3}\left(\frac{2\pi c_s{}^2\hbar^2}{m-2}\right)^{3/m}I\frac{\Omega k_B}{c_s}\Delta T(aN\sigma)^{-3/m}, \quad (5.6)$$

where I is a constant given by (B11). Comparison of (5.6) with the momentum density obtained from

numerical calculations with $m=4$ in the high-impurity limit gives a value of $I=2.23$. The dependence of the momentum in Eq. (5.6) on the impurity concentration agrees with that obtained from the numerical integration to be discussed. In view of (5.1), the thermal conductivity will have the following dependencies: $\kappa \propto a^{1-3/m}(N\sigma)^{-3/m}$, independent of ΔT and T.

To find the momentum density in the low-impurity-scattering limit, we integrate (5.5) over μ. This yields

$$P=2\pi\Omega\hbar\int_0^\infty C^0k^3\{\tfrac{1}{2}-\xi k^m \times[1-\xi k^m\ln(1+1/\xi k^m)]\}dk. \quad (5.7)$$

In the low-impurity limit, the integrand has a pronounced maximum for a value k_1 of the momentum, such that $\xi k_1{}^m\ll 1$. In this limit,

$$P=2\pi\Omega\hbar\int_0^\infty C^0k^3(\tfrac{1}{2}-\xi k^m)dk=2\pi\Omega\hbar\left(\frac{k_B}{c_s\hbar}\right)^4 \times\left[\tfrac{1}{2}J_3(T_1{}^4-T_2{}^4)-\xi\left(\frac{k_B}{c_s\hbar}\right)^m J_{m+3}(T_1{}^{m+4}-T_2{}^{m+4})\right], \quad (5.8)$$

where J_n is defined in terms of the Riemann ζ function by

$$J_n=\int_0^\infty \frac{x^n dx}{e^x-1}=n!\zeta(n+1). \quad (5.9)$$

For $\Delta T/T_m\ll 1$, (5.8) reduces to

$$P=4\pi\Omega\hbar J_3\left(\frac{k_BT_m}{c_s\hbar}\right)^4\frac{\Delta T}{T_m}\left[1-\frac{m+4}{2}\frac{J_{m+3}}{J_3} \times\left(\frac{aN\sigma}{\pi c_s{}^2\hbar^2}\right)\left(\frac{k_BT_m}{c_s\hbar}\right)^m\right] \quad (5.10)$$

in agreement with Ref. 5. The reader will notice, that the momentum density P, as given in (5.10), becomes negative at some value of the temperature T_m. This is obviously incorrect, and is due to the neglect of the last (logarithmic) term in (5.7). (See also the discussion of Fig. 8.)

Energy Density and Temperature

Having obtained the momentum density [and heat flux (5.1)] we proceed to evaluate the *energy density* $E(x)$ and temperature $T(x)$ at an arbitrary point x in the slab. The phonon energy density is

$$E(x)=\Omega\int \epsilon_k f_k(x)d^3k. \quad (5.11)$$

Using f^0 and g_0, and carrying out the μ integration yields

$$E(x)=E_0-2\pi\Omega c_s\hbar\frac{x}{a}\int_0^\infty C^0\xi k^{m+3}\ln(1+1/\xi k^m)dk, \quad (5.12)$$

where

$$E_0=2\pi\Omega c_s\hbar J_3(k_B/c_s\hbar)^4(T_1{}^4+T_2{}^4). \quad (5.13)$$

In the high-impurity limit the peak of the integrand is such that $\xi k_1{}^m\gg 1$. In all the region of integration where the integrand is appreciable, $\xi k^m>1$. Therefore, the logarithm may be expanded, and we obtain

$$E(x)=E_0-2\pi\Omega c_s\hbar\frac{x}{a}\int_0^\infty C^0k^3dk. \quad (5.14)$$

For $\Delta T/T_m\ll 1$ use of (5.13) and (B3) of the Appendix gives

$$E(x)=4\pi\Omega c_s\hbar J_3(k_BT_m/c_s\hbar)^4 \times[1-2(\Delta T/T_m)(x/a)]. \quad (5.15)$$

The *temperature* at any point x in the slab is defined by Ref. 5 as

$$T(x)=\frac{c_s\hbar}{k_B}\left[\frac{E(x)}{4\pi\Omega c_s\hbar J_3}\right]^{1/4}. \quad (5.16)$$

From (5.15), we have for $\Delta T/T_m\ll 1$

$$T(x)=T_m-(x/a)\tfrac{1}{2}\Delta T. \quad (5.17)$$

In the high-impurity-concentration region the temperature varies linearly from $T(-a)=T_1$ to $T(a)=T_2$, crossing the mean temperature T_m at the center of the slab. For the low-impurity region the second term in (5.12) becomes negligible and the energy approaches E_0; consequently, the corresponding temperature approaches the mean temperature T_m at all points in the slab. Section VI deals with intermediate-impurity concentrations.

VI. NUMERICAL SOLUTION

In an attempt to solve Eq. (3.15) for all impurity concentrations, we formulate a numerical method based on a finite difference approach of Mennig and Marti.[7] This approach was originally developed to handle finite multilayer slabs, cells, and shielding problems in neutron transport theory, involving rather general boundary conditions. To our knowledge, the method has not been used previously in an actual problem: The following sections will show that its use is very convenient and its convergence properties are satisfactory.

[7] J. Mennig and J. Marti, Technische Mitteilung PH-257, Eidg. Institut für Reaktorforschung, Würenlingen, AG, Switzerland, 1966 (unpublished). A full account of the numerical method, including applications to neutron and phonon transport, will be published shortly, jointly with these authors.

Description of the Finite Difference Method

The Boltzmann transport equation is discretized in the space variable x, whereas the angular part is treated analytically. Discretization of Eq. (3.15) is achieved by assuming that the value of $f_k{}^1(x_{i+1/2})$ at a space point $x_{i+1/2}$ can be replaced by its average value $\frac{1}{2}(f_i{}^1+f_{i-1}{}^1)$ in the interval (x_i, x_{i-1}). (We omit the wave-number variable k in the sequel—the subscripts refer to the discrete coordinate points.) It follows that

$$f_i{}^1=\left(\frac{\mu-\beta}{\mu+\beta}\right)f_{i-1}{}^1+\frac{1}{2}\frac{\beta}{\mu+\beta}[\Phi_i+\Phi_{i-1}-2C^0S(\mu)]$$
$$\text{for} \quad i=2, \ldots, n, \quad (6.1)$$

where

$$\Phi_l=\int_{-1}^{1} f_l{}^1(x_l,k,\mu')d\mu',$$

$$\Delta=x_i-x_{i-1},$$

and

$$\beta=\frac{\Delta}{4\Lambda(k)a}.$$

Up to the factor c_s, the quantities Φ_l represent the additional flux of phonons at the point x_l in the slab due to the presence of scattering centers.

Separating (6.1) into a coupled set of equations by using the definition (3.16) gives

$$f_i{}^+=\left(\frac{\mu-\beta}{\mu+\beta}\right)f_{i-1}{}^++\frac{1}{2}\frac{\beta}{\mu+\beta}[\Phi_i+\Phi_{i-1}-2C^0]$$
$$\text{for} \quad \mu>0, i=2, \ldots, n \quad (6.2)$$

and

$$f_{i-1}{}^-=\left(\frac{\tilde{\mu}-\beta}{\tilde{\mu}+\beta}\right)f_i{}^-+\frac{1}{2}\frac{\beta}{\tilde{\mu}+\beta}[\Phi_i+\Phi_{i-1}+2C^0]$$
$$\text{for} \quad \tilde{\mu}>0, i=2, \ldots, n. \quad (6.3)$$

Equations (6.2) and (6.3) constitute a set of $2(n-1)$ linear integral equations in $2n$, unknowns $f_1{}^+$, ..., $f_n{}^+$ and $f_1{}^-$, ..., $f_n{}^-$. The remaining two unknowns are determined by the boundary conditions (3.12) which are satisfied by

$$f_1{}^+=0 \quad \text{for} \quad 0<\mu\leq 1 \quad (6.4)$$

and

$$f_n{}^-=0 \quad \text{for} \quad 0<\tilde{\mu}\leq 1. \quad (6.5)$$

To find $f_i{}^+$, we substitute successively $f_j{}^+$ for $j=2, 3, \cdots, i-1$ into Eq. (6.2) and use Eq. (6.4). This gives

$$f_i{}^+=\frac{1}{2}\frac{\beta}{\mu+\beta}\sum_{l=1}^{i-1}\left(\frac{\mu-\beta}{\mu+\beta}\right)^{i-l-1}[\Phi_l+\Phi_{l+1}-2C^0]$$
$$\text{for} \quad \mu>0, i=2, \ldots, n. \quad (6.6)$$

Similarly, to find $f_i{}^-$, we substitute successively $f_j{}^-$ for $j=n, n-1, \cdots, i+1$ into Eq. (6.3) and use Eq. (6.5). This gives

$$f_i{}^-=\frac{1}{2}\frac{\beta}{\tilde{\mu}+\beta}\sum_{l=1}^{n-i}\left(\frac{\tilde{\mu}-\beta}{\tilde{\mu}+\beta}\right)^{n-i-l}[\Phi_{n-l}+\Phi_{n+1-l}+2C^0]$$
$$\text{for} \quad \tilde{\mu}>0, i=1, \ldots, n-1. \quad (6.7)$$

Equations (6.6) and (6.7) give, respectively, the contributions to the phonon distribution function due to forward and backward impurity scattering.

At this point, we have succeeded in expressing the distribution function $f^{\pm}$ entirely in terms of the fluxes. The remaining part of the development deals with the determination of the fluxes by deriving a system of linear equations for them. This set will no longer involve the distribution function.

Determination of the Fluxes

In order to determine the flux Φ_i at each point x_i, we write

$$\Phi_i=\int_{-1}^{1} f_i{}^1(\mu')d\mu'=\int_0^1 (f_i{}^++f_i{}^-)d\mu'$$
$$\text{for} \quad i=1, \ldots, n. \quad (6.8)$$

We define

$$\eta=(\mu-\beta)/(\mu+\beta) \quad (6.9)$$

and

$$Z_j=\int_{-1}^{(1-\beta)/(1+\beta)}\frac{\eta^{j-1}}{1-\eta}d\eta \quad \text{for} \quad j=1, \ldots, n. \quad (6.10)$$

Z_j satisfies the recursion relation

$$Z_j=\frac{1}{j-1}\left[(-1)^{j-1}-\left(\frac{1-\beta}{1+\beta}\right)^{j-1}\right]+Z_{j-1}$$
$$\text{for} \quad j=2, \ldots, n. \quad (6.11)$$

Substitution of $f_i{}^+$ and $f_i{}^-$ from Eq. (6.6) and (6.7) into (6.8), and integration over μ' yields a set of linear-algebraic equations which can be written in concise form as

$$\sum_{l=1}^{n}(\delta_{i,l}-M_{i,l})\Phi_l=S_i \quad \text{for} \quad i=1, \ldots, n. \quad (6.12)$$

With the notation

$$\Theta_{i,l}=1 \quad \text{for} \quad i\geq l,$$
$$=0 \quad \text{for} \quad i<l, \quad (6.13)$$

the matrix elements are

$$M_{i,l}=\tfrac{1}{2}\beta[(1-\delta_{l,n})(\Theta_{i,l+1}Z_{i-l}+\Theta_{l,i}Z_{l+1-i})$$
$$+(1-\delta_{l,1})(\Theta_{i,l}Z_{i+1-l}+\Theta_{l-1,i}Z_{l-i})]$$
$$\text{for} \quad i=1, \ldots, n, \; l=1, \ldots, n. \quad (6.14)$$

The inhomogeneous terms of Eqs. (6.12) are

$$S_i=\beta C^0\sum_{l=1}^{n}(\Theta_{l,i}Z_{l+1-i}-\Theta_{i,l+1}Z_{i-l}),\quad i=1,\ldots,n. \quad (6.15)$$

The dimension of the matrix which determines the fluxes is equal to the number of discretization points. Therefore, the matrix inversion time (i.e., the time needed to solve for the fluxes) is proportaional to n^3 for Gaussian elimination. This we used in combination with an iterative improvement in the electronic computational solution of the linear equation (6.12). It was found most practical to limit the dimension of the matrix to 23.

Reduction of the Matrix Dimensions

Two facts make it possible to solve the problem accurately using 46 discretization points. First, the dimension of the matrix $M_{i,l}$ can be reduced to $n/2$—half the number of discretization points (we use $n=$even). Second, the spatial derivative of the scattering contribution to the phonon distribution function does not vary rapidly: We recall that $g_0^{\pm}$ is linear in x for both high- and low-impurity-scattering limits. Only in a small solid angle around $\mu=0$, near $x=\pm a$, for the middle-impurity region does the spatial derivative vary so rapidly that 46 points would not resolve the function. The reduction of the matrix reduction of the matrix dimensions $M_{i,l}$ is accomplished by examination of Eqs. (6.14) and (6.15). The following properties are observed:

$$M_{n+1-i,n+1-l}=M_{i,l} \text{ for } i=1,\ldots,n, l=1,\ldots,n \quad (6.16)$$

and

$$S_{n+1-i}=-S_i \quad \text{for} \quad i=1,\ldots,n. \quad (6.17)$$

Using (6.16), and (6.17) and the matrix Eq. (6.12), it can be proven that the fluxes satisfy the following relation:

$$\Phi_{n+1-l}=-\Phi_l \quad \text{for} \quad l=1,\ldots,n. \quad (6.18)$$

The original set of n equations (6.12) can now be reduced to a set of $n/2$ equations of the form

$$\sum_{l=1}^{n/2}R_{i,l}\Phi_l=S_i \quad \text{for} \quad i=1,\ldots,n/2, \quad (6.19)$$

where we have set

$$R_{i,l}=\delta_{i,l}-M_{i,l}+M_{i,n+1-l} \quad \text{for} \quad i=1,\ldots,n/2,\ l=1,\ldots,n/2. \quad (6.20)$$

In impurity-concentration regions where $\beta<3\times10^3$, the above form of the matrix elements $R_{i,l}$ was used for numerical computation. For $\beta>3\times10^3$ [i.e., the free path $\lambda(k)<\frac{1}{6}\times10^{-3}\Delta$, where $\Delta=$discretization interval] expansions of the matrix elements $R_{i,l}$ and of S_i were carried out analytically in inverse powers of β, up to order β^{-2}. These expansions are necessary, since the matrix $R_{i,l}$ is singular to order β^{-1} for large β.

VII. MOMENTUM AND ENERGY DENSITIES CALCULATED FROM THE NUMERICAL SOLUTION

We should like to emphasize that even with the present-day high-speed large-memory computers an accurate solution of the Boltzmann integro-differential equation was, for us, a difficult task. Only by the use of numerous *ad hoc* mathematical expansions and other "tricks" was the final accuracy gradually achieved. The present section is meant to provide the reader with a sampling of those difficulties, by giving a more detailed account of the method of calculation of the phonon momentum density and energy density.

Momentum Density (Numerical)

The total momentum density at each space point x_i is

$$P_i=P_0+\Omega\int\hbar k\mu f_i^1 d^3k. \quad (7.1)$$

P_0 would be the momentum density if there were no impurities. From (5.8) we have

$$P_0=\pi\hbar\Omega J_3(k_B/c_s\hbar)^4(T_1^4-T_2^4). \quad (7.2)$$

Substituting the discretized solutions f_i^+ and f_i^- given by (6.6) and (6.7) into (7.1) and integrating over the angular variables yields

$$P_i=P_0+\pi\Omega\hbar\int_0^{\infty}k^3\Big[(1-\delta_{i,1})\sum_{l=1}^{i-1}\beta^2(Q_{i-l}+Q_{i-l+1})\times(\Phi_l+\Phi_{l+1}-2C^0)-(1-\delta_{i,n})\sum_{l=1}^{n-i}\beta^2(Q_{n-i-l+1}+Q_{n-i-l+2})\times(\Phi_{n-l}+\Phi_{n-l+1}+2C^0)\Big]dk. \quad (7.3)$$

The quantities Q_m are defined in terms of Z_m as

$$Q_m=\int_{-1}^{(1-\beta/1+\beta)}\frac{\eta^{m-1}d\eta}{(1-\eta)^2}=\left(\frac{1-\beta}{1+\beta}\right)^{m-1}\Big/\left(1-\frac{1-\beta}{1+\beta}\right)-\tfrac{1}{2}(-1)^{m-1}-(m-1)Z_{m-1} \quad \text{for} \quad m=2,\ldots,n \quad (7.4)$$

and

$$Q_1=1/2\beta. \quad (7.5)$$

Initially Eq. (7.3) was the form used to find the total momentum density in all the impurity regions by numerically integrating the second term over k and then adding P_0 to it. The result was inaccurate for very small free-path ratios for two reasons: First, the matrix elements were not calculated accurately, prior to the $1/\beta^2$ expansion (see end of Sec. VI). Second, since the

momentum density approaches zero in the high-impurity (zero free path) limit, the integration must give a second term equal to $-P_0$ in this limit. However, this did not occur because the integral J_3 in P_0 was taken from a table of Riemann ζ functions which was not sufficiently accurate; therefore, the momentum density levelled off at 10^{-10} for $T_m=1°\mathrm{K}$.

The expansion of the matrix elements and of the inhomogeneous terms in power of β^{-1} solved the first problem by giving accurate fluxes Φ_i at each point. The second problem was eliminated by a $1/\beta^2$ expansion of $\beta^2 Q_j$, which made it possible to extract the $-P_0$ term from the integral in (7.3). The total momentum density at the position x_i can now be written as

$$P_i=\pi\Omega\hbar\int_0^\infty k^3\beta^2\{(1-\delta_{i,1})\sum_{l=1}^{i-1}[(Q_{i-l}+Q_{i-l+1})(\Phi_l+\Phi_{l+1}) -2C^0(Q_{i-l}'+Q_{i-l+1}')]-(1-\delta_{i,n}) \times\sum_{l=1}^{n-i}[(Q_{n-i-l+1}+Q_{n-i-l+2})(\Phi_{n-l}+\Phi_{n-l+1}) +2C^0(Q_{n-i-l+1}'+Q_{n-i-l+2}')]\}dk, \quad (7.6)$$

where

$$\beta^2(Q_m'+Q_{m+1}')=\beta^2(Q_m+Q_{m+1})+(-1)^m/2. \quad (7.7)$$

Equation (7.6) is programmed to obtain the numerical results.

Energy Density (Numerical)

The energy density E_i of the phonons at the position x_i in the slab is found by substituting f_i^+ and f_i^- into the integral (5.11) and integrating over the angular variables. This gives

$$E_i=E_0+\pi\Omega C_s\hbar\int_0^\infty k^3[(1-\delta_{i,1})\sum_{l=1}^{i-1}\beta P_{i-l}(\Phi_l+\Phi_{l+1}-2C_0) +(1-\delta_{i,n})\sum_{l=1}^{n-i}\beta P_{n-i-l+1}(\Phi_{n-l}+\Phi_{n-l+1}+2C_0)]dk, \quad (7.8)$$

with E_0 given by (5.13). The temperature $T(x_i)$ is calculated from E_i using (5.16).

The numerical calculations were performed on an electronic digital computer.[8] A computer program consisting of a main program and five subroutines was written in the programming language FORTRAN IV[9] in order to calculate the discretized solutions f_i^+ and f_i^- derived in Sec. VI and to carry out the necessary k-space integrations to find the momentum and the energy at each discretization point x_i in the slab.

The main program contains loops for varying all the relevant parameters of the problem, such as the sound velocity c_s, the impurity concentration times scattering cross section $N\sigma$ (the free-path ratio Λ), the angular variable μ, the mean temperature T_m, and the temperature difference ΔT.

The set of linear equations (6.19) is solved by a Gaussian elimination with partial pivoting.[10] A relaxation algorithm improves the solutions, using as a first approximation the results obtained from the Gaussian elimination. These solutions are found for every value k of the wave vector, for which the distribution function is needed for accurate integration. For an accuracy of 10^{-6} a maximum of 257 values of k are needed. The necessary integrations to obtain energy and momentum densities are carried out by means of a Romberg algorithm.[11]

To compute the phonon distribution function, the momentum, the energy, and the number of particles at each discretization point x_i (out of n) for 13 values of μ and for fixed values of the parameters c_s, $N\sigma$ (or Λ), T_m, and ΔT, the following approximate times were observed: 25–50 sec for $n=10$, 430 sec for $n=28$, and 1400 sec for $n=46$.

VIII. RESULTS AND DISCUSSION

This section contains the results obtained by the numerical methods. The results obtained by analytical methods (cf. Sec. IV) are, with the exception of two figures, not separately displayed because, within the limits of drafting accuracy, they coincide with the numerical results.

Spatial and Directional Distribution of Phonons

Figures 2–6 represent various results concerning the phonon distribution function. The distribution function has been written as a sum of two Bose distributions at temperatures $T_m+\frac{1}{2}\Delta T$ and $T_m-\frac{1}{2}\Delta T$ [see (2.3)] and a function $f_1^{\pm}$. The superscript $\pm$ denotes the sign of the phonon velocity component along the x axis. Each of the Bose distributions is isotropic in one-half of the solid angle, zero in the other half, and they are independent of x. The function $f_1^{\pm}$ depends on the angle α between the phonon's direction of propagation and the x axis, as well as on x, for every value of the wave number k, and the parameters of the problem.

The relief diagrams [Fig. 2(a)–2(c)] show clearly how the free path ratio Λ affects the distribution function f. When the free path of the phonons of wave vector k is much smaller than the slab thickness [Fig. 2(a)], the phonon distribution varies linearly across the slab—more phonons per unit volume being

[8] Model 6400 Computer of the Control Data Corporation, S. Minneapolis, Minn. 55420, at the Florida State University. The assistance rendered by the U. S. National Science Foundation through its grant GJ 367 to the Computing Center of the Forida State University is gratefully acknowledged.

[9] American Standards Association Proposed Standards for FORTRAN, Comm. Assoc. Comp. Mach. 7, 591 (1964); 8, 287 (1965).

[10] G. Forsythe and C. B. Moler, in *Series in Automatic Computation* (Prentice-Hall, Inc., Englewood Cliffs, New Jersey, 1967).

[11] F. L. Bauer, E. Stiefel, and H. Rutishauser, in *Proceedings of the Symposium in Applied Mathematics*, edited by N. Metropolis (American Mathematical Society, Providence, R. I., 1963), Vol. 15, p. 199.

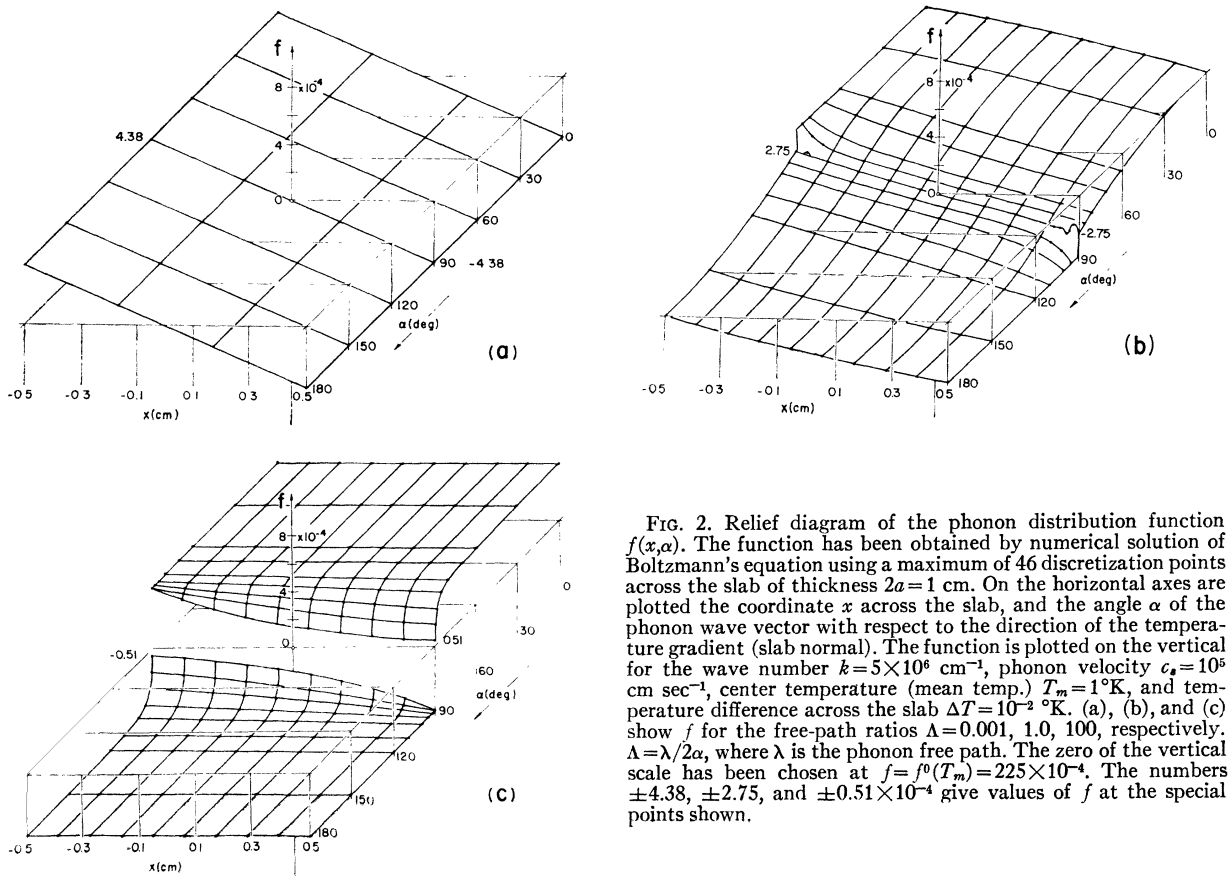

FIG. 2. Relief diagram of the phonon distribution function $f(x,\alpha)$. The function has been obtained by numerical solution of Boltzmann's equation using a maximum of 46 discretization points across the slab of thickness $2a=1$ cm. On the horizontal axes are plotted the coordinate x across the slab, and the angle α of the phonon wave vector with respect to the direction of the temperature gradient (slab normal). The function is plotted on the vertical for the wave number $k=5\times10^6$ cm^{-1}, phonon velocity $c_s=10^5$ cm sec^{-1}, center temperature (mean temp.) $T_m=1$°K, and temperature difference across the slab $\Delta T=10^{-2}$ °K. (a), (b), and (c) show f for the free-path ratios $\Lambda=0.001$, 1.0, 100, respectively. $\Lambda=\lambda/2\alpha$, where λ is the phonon free path. The zero of the vertical scale has been chosen at $f=f^0(T_m)=225\times10^{-4}$. The numbers ±4.38, ±2.75, and $\pm0.51\times10^{-4}$ give values of f at the special points shown.

found at the hotter parts of the slab. The distribution function does not vary with the angle hence, is isotropic.

As the free path of this particular group of phonons (characterized by its wave number k) approaches and finally exceeds the slab thickness [Fig. 2(b), and 2(c), respectively] the distribution function varies less and less along the x axis, but varies more and more with the angle α of phonon propagation direction with respect to this axis. In particular, we see in Fig. 2(c), that at $\alpha=0°$ and at $\alpha=180°$ the distribution function is practically the same, as the one corresponding to the sum of the two Bose distributions emitted by the reservoirs into the slabs at temperatures $T_m+\frac{1}{2}\Delta T$ and $T_m-\frac{1}{2}\Delta T$, respectively.[12] For angles $\alpha\simeq90°$, the impurity scattering smooths out the difference between these two Bose distributions. Note, that phonons travelling at angles close to $\alpha\simeq90°$ travel much longer paths in the slab, than those at $\alpha=0$ or 180°, hence, for them scattering is more effective.

The distribution function f in the relief diagram Fig. 2(b) exhibits an anomaly at $x=\pm0.5$ cm, $\alpha=90°$. The oscillatory anomaly displayed is due to the bad convergence of the numerical calculation around 90°, and can only be diminished by increasing the number n of discretization points in the finite-difference method used.

This conclusion is born out by Fig. 3. Here f_1^- is plotted as a function of x for $\alpha=90.5°$. The oscillations of f_1^- diminish and disappear (except for $x\simeq0.5$ cm) as the number of discretization points is increased. The maximum value $n=46$ represents a compromise between excessive computer time use and acceptable accuracy.

To test the accuracy of the analytic solution obtained in Sec. IV, we plotted the first analytic approximation g_0 and the second analytic approximation g_0+g_1 together with the numerically obtained f_1^- as a function of x in Fig. 4. The three functions are plotted for such values of the parameters, for which the analytic approximations are expected to be bad. The free path is of the order of ten times the slab thickness and the phonons move at a grazing angle ($\alpha=95°$) with respect to the slab boundaries. Despite these adverse conditions, the analytic approximations are seen to be quite satisfactory.

As noted with reference to the relief diagrams the distribution function is strongly changed by scattering at grazing angles of phonon propagation. This fact is particularly born out by Fig. 5. Here f_1^- is plotted *versus* α for fixed values of k and x, with the free-path

[12] The latter distribution, which prevails in the total absence of scatterers, is not shown in Fig. 2(c). It would be represented by the two horizontal planes at $f=4.38\times10^{-4}$ for $\alpha<90°$, and at $f=-4.38\times10^{-4}$ for $\alpha>90°$.

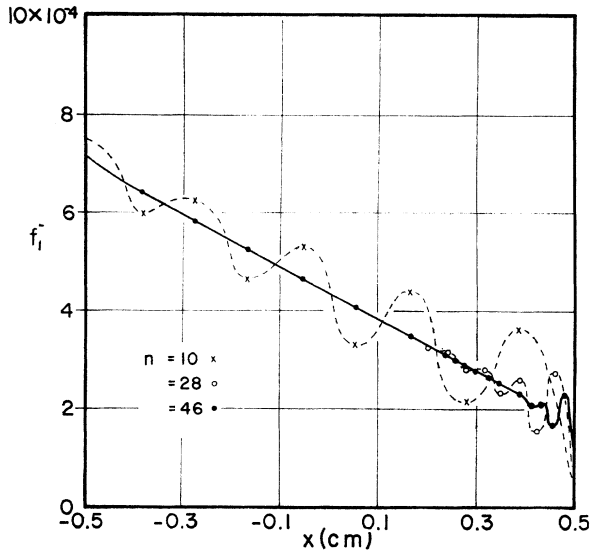

FIG. 3. Influence of the number of discretization points n on the computational accuracy of the function f_1^- defined in the text. The function f_1^- is plotted versus the coordinate x across the slab. for the same set of parameters used in Fig. 2, and $\Lambda=1.0$. The phonons move at the angle $\alpha=90.5°$, almost parallel to the slab boundary. The plot smooths out as n is increased from 10 to 28 to 46, respectively.

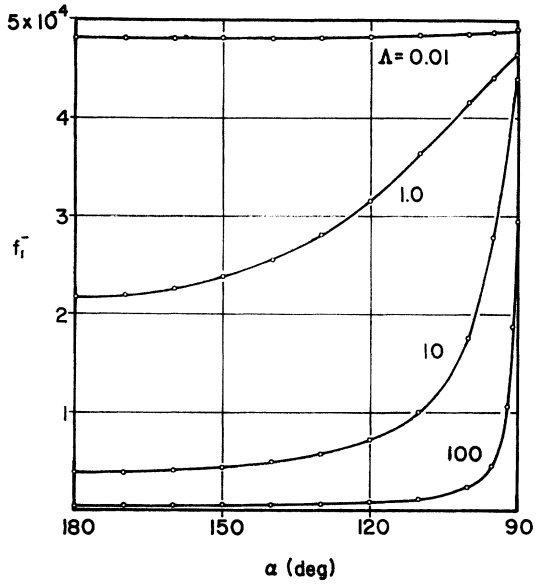

FIG. 5. Dependence of the correction f_1^- to the Bose-distribution function on the phonon propagation angle $\alpha=\sphericalangle(\mathbf{k},x)$. The four curves represent results for different free-path ratios Λ, for the point $x=-0.056$ cm in the slab of 1 cm thickness. Discretization parameters $n=10$–46 have been used. The other parameters are as in Fig. 2.

ratio as a parameter. For long free paths the distribution function is only affected for α close to 90°. For short free paths the distribution function becomes isotropic.

When the free-path ratio Λ is much smaller than unity, a distribution is established at the point x in the slab which differs only infinitesimally from a drifting Bose distribution with temperature $T(x)=T_1-[(a+x)/2a]\Delta T$. Hence, the function f_1^- approaches the limit

$$\lim_{\Lambda\to 0} f_1^-(x)=f^0(T(x))-f^0(T_2)$$
$$=-[f^0(T_1)-f^0(T_2)][(x-a)/2a]. \quad (8.1)$$

For the parameters used in Fig. 5, this limiting value is $f_1^-(-0.056\text{ cm})=4.87\times10^{-4}$, and is 99% attained for $\Lambda\leq 0.01$.

Figure 6 shows how the phonon distribution approaches the drifting Bose distribution as a function of the free-path ratio. Let us consider the drifting Bose distribution to be attained when the deviation from it is smaller than 1% of the deviation which exists for a slab with no scattering centers. It may be seen then from Fig. 6, that this condition is attained for $\Lambda\simeq 0.1$ ($N\sigma\simeq 10^{-69}$). For smaller free-path ratios the distribution function

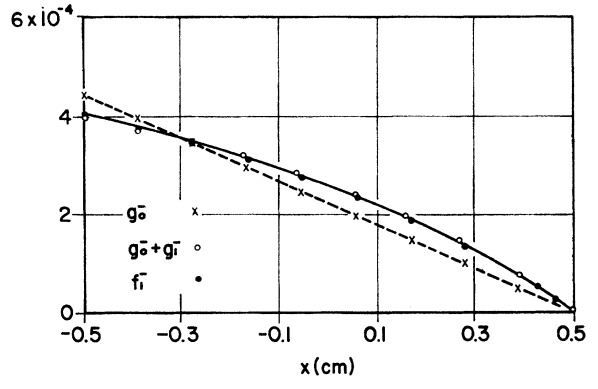

FIG. 4. Comparison of the accuracy of the analytical and the numerical solutions. Plotted as functions of the coordinate x across the slab are g_0^-, $g_0^-+g_1^-$, f_1^- defined in the text. The parameters are the same as in Fig. 2, $\Lambda=10$ and $\alpha=95°$. It can be seen that $g_0^-+g_1^-$ approximates the numerically obtained function f_1^- quite well.

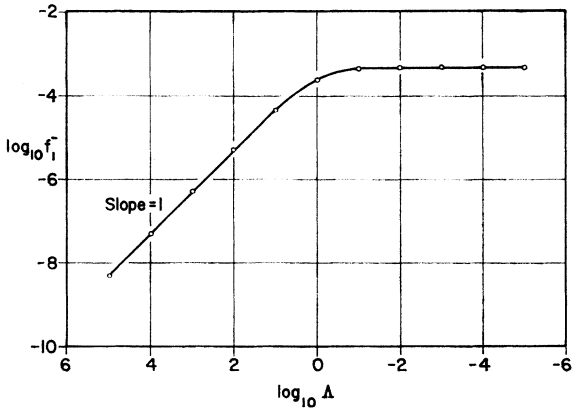

FIG. 6. Dependence of the correction f_1^- to the Bose-distribution function on the free-path ratio Λ. The log-log plot shows both numerical and analytical results (coincident within plot accuracy) for a slab of thickness 1 cm at the point $x=-0.056$ cm and a propagation angle $\alpha=150°$. The other parameters are as in Fig. 2.

does not undergo further changes (horizontal part of the curve).

On the other hand, we may say that the distribution function is not affected by the scattering if it still deviates by more than 99% from $f^0(T(x))$. Figure 6 shows, that this is the case for $\Lambda > 100 (N\sigma < 10^{-72})$. Hence we see, that the drastic changes in the distribution function occur in the range

$$0.1 < \Lambda < 100.$$

From these considerations (and remembering that $\mu^{-1} = 1.16$) we derive the rule-of-thumb that *when a phonon is scattered more than 12 times on the average, the equilibrium distribution is attained to 99%.*

Let us turn to the analysis of the heat flux which is a result of the anisotropy of the phonon distribution function. We plot the phonon momentum density $P = c_s^{-2} Q$, where Q is the heat flux due to phonons belonging to one of the three polarization branches.

Variation of Heat Flux and Thermal Conductivity

Figure 7 shows the dependence of the momentum density on the free-path ratio, for different slab-center temperatures T_m. For large free-path ratio, the momentum density is at first independent of the free-path ratio. In this region, the phonons move freely from one boundary to the other, and the heat current is limited only by the fact, that the boundaries emit a finite number of phonons per unit time into the slab.

Let us focus attention on the curve for $T_m = 1°\text{K}$ of Fig. 7. For this temperature, the momentum integrand (7.6) peaks at a certain value k_1 of the wave number. These phonons at the peak are the ones whose free-path ratio $\Lambda = \Lambda(k_1)$ is used as the abscissa of the figure. (We recall that the scattering cross section, and therefore Λ, depends on k.) A noticeable decrease of the momentum density occurs as $\Lambda(k_1)$ becomes smaller that 1.0. *As soon as* $\Lambda(k_1) < 10^{-4}$ *the dependence of the momentum density on the free-path ratio may be described by a simple power law* $P \propto \Lambda^{3/4}$. This means that the heat flux becomes proportional to the $-\frac{3}{4}$ power of the impurity concentration.

Retracing the origin of this dependence, we find, that in general the law is $-3/m$, where m is the power of k which occurs in the relation [cf. Appendix Eq. (A12)]

$$s_k \propto k^m.$$

Scattering theory predicts $m = 4$ for punctual, $m = 3$ for linear, and $m = 2$ for planar scatterers. Hence, we expect $P \propto \Lambda$ for linear, and $P \propto \Lambda^{3/2}$ for planar scatterers in the limit of $\Lambda \ll 1$.

Turning now to the curves for $T_m = 0.1°\text{K}$ and $T_m = 10°\text{K}$ of Fig. 7, we see that the onset of the decrease

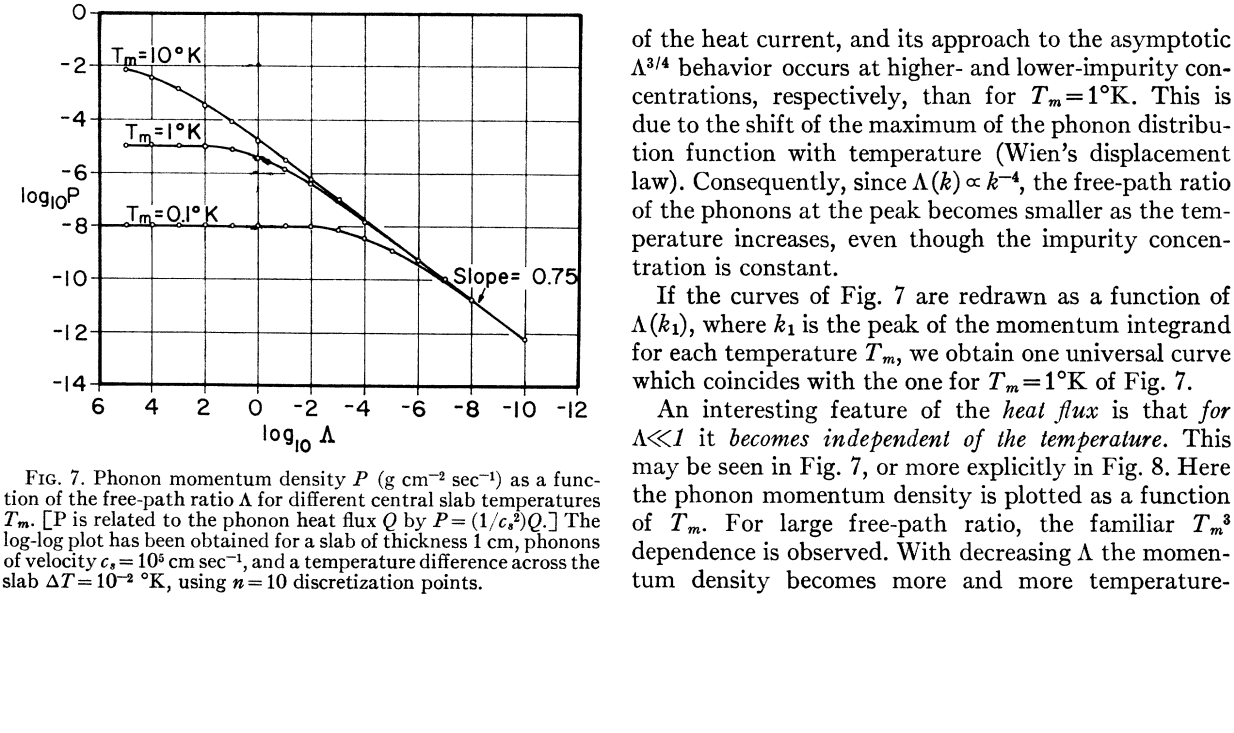

FIG. 7. Phonon momentum density P (g cm^{-2} sec^{-1}) as a function of the free-path ratio Λ for different central slab temperatures T_m. [P is related to the phonon heat flux Q by $P = (1/c_s^2)Q$.] The log-log plot has been obtained for a slab of thickness 1 cm, phonons of velocity $c_s = 10^5$ cm sec^{-1}, and a temperature difference across the slab $\Delta T = 10^{-2}$ °K, using $n = 10$ discretization points.

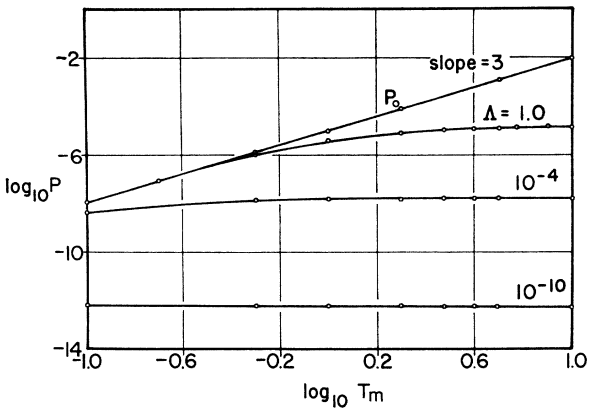

FIG. 8. Phonon momentum density P (g cm^{-2} sec^{-1}) as a function of the mean temperature T_m(°K), for different free-path ratios Λ. The other parameters of the log-log plot are as in Fig. 7.

of the heat current, and its approach to the asymptotic $\Lambda^{3/4}$ behavior occurs at higher- and lower-impurity concentrations, respectively, than for $T_m = 1°\text{K}$. This is due to the shift of the maximum of the phonon distribution function with temperature (Wien's displacement law). Consequently, since $\Lambda(k) \propto k^{-4}$, the free-path ratio of the phonons at the peak becomes smaller as the temperature increases, even though the impurity concentration is constant.

If the curves of Fig. 7 are redrawn as a function of $\Lambda(k_1)$, where k_1 is the peak of the momentum integrand for each temperature T_m, we obtain one universal curve which coincides with the one for $T_m = 1°\text{K}$ of Fig. 7.

An interesting feature of the *heat flux* is that *for* $\Lambda \ll 1$ it *becomes independent of the temperature.* This may be seen in Fig. 7, or more explicitly in Fig. 8. Here the phonon momentum density is plotted as a function of T_m. For large free-path ratio, the familiar T_m^3 dependence is observed. With decreasing Λ the momentum density becomes more and more temperature-

independent, and for $\Lambda=10^{-8}$ there is no noticeable change of heat flux over the range of $T_m=0.1°K$ to $T_m=10°K$. For all these curves, the temperature difference across the slab is $\Delta T=10^{-2}°K$. The temperature independence of the thermal conductivity for materials with short phonon mean free path has been observed, for instance, in diamond[13] and isotopic mixtures of solid helium.[14]

Since the momentum density P is proportional to the thermal conductivity κ, Fig. 8 may also be viewed as the familiar plot of thermal conductivity versus temperature. (Note the log-log scale.) Experimental plots usually exhibit a rise with slope corresponding to $\kappa \propto T_m^3$, go through a maximum, then fall again. The curves of Fig. 8 do rise with the expected slope at low temperatures, but then level off to a temperature-independent maximum, and do not decline. This behavior is in contrast to the analytical result given in (5.10). The latter is identical to the well-known result obtained in the relaxation-time approximation,[1] and does exhibit a maximum of the thermal conductivity (at some temperature T_0) followed by a decline, and finally becomes negative at $\sim 1.3T_0$.

Relaxation-time theory was used by other authors to identify the theoretically obtained maximum with the experimentally observed peak.[1] However, the maximum exhibited by the approximate formula (5.10)—which is the same as the formula given by relaxation-time theory—is entirely spurious. It is clear, that the low-impurity approximation has broken down when it yields a negative thermal conductivity at $1.3T_0$. *Our results show, that the low-impurity approximation is incorrect at and above* T_0. This is born out by the numerical results presented in Fig. 8 and is discussed mathematically in Sec. V. The experimentally observed maximum has no relation to the impurity scattering, but is entirely due to the onset of phonon-phonon scattering. Figure 9 shows in more detail the deviation of the heat flux from the T_m^3 behavior. Here P/T_m^3 is plotted as a function of T_m. In the absence of scattering there results a horizontal line.

The dependency of the thermal conductivity on impurity concentration, slab thickness, and temperature may be understood by a qualitative argument, originally due to Pomeranchuk.[15] Let us express the thermal conductivity κ in the form

$$\kappa=\Omega\int_{k_0}^{\infty}\lambda_k dC_k. \tag{8.2}$$

Here λ_k is the free path of phonons of wave number k, dC_k is the specific heat of phonons with wave vectors in a volume element d^3k of wave-vector space. The crucial point of the argument is that the lower limit k_0 of the integral is provided by the phonons, whose free path is equal to the thickness of the slab

$$\lambda_{k_0}=2a. \tag{8.3}$$

We can argue in a crude fashion, that this is so, because phonons with a scattering free path larger than $2a$ have an effective free path determined by the slab dimensions. We note (see Appendix A) that for Rayleigh scattering

$$\lambda_k \propto N^{-1}k^{-4}, \tag{8.4}$$

hence, combining (8.3) and (8.4) we have

$$k_0 \propto (aN)^{-1/4}. \tag{8.5}$$

On the other hand, the specific heat is related to the energy density through

$$dC_k=\frac{\partial}{\partial T}(\epsilon_k f^0)d^3k \propto k^3 dk\frac{\partial}{\partial T}f^0 \propto -T^{-1}k^4 dk\frac{\partial f^0}{\partial k}. \tag{8.6}$$

Inserting (8.4) and (8.6) into (8.2) we find

$$\kappa \propto -N^{-1}T^{-1}\int_{k_0}^{\infty}\frac{\partial f^0}{\partial k}dk=N^{-1}T^{-1}f^0|_{k=k_0}. \tag{8.7}$$

In the high-impurity-concentration limit $k_BT/c\hbar k_0 \ll 1$, and we may write for the Bose distribution

$$f^0|_{k=k_0}=k_BT/c\hbar k_0 \propto T(aN)^{1/4}. \tag{8.8}$$

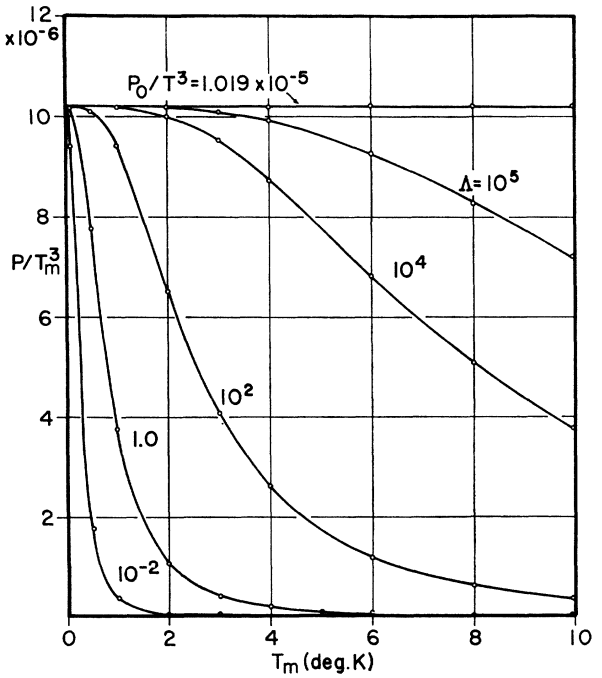

FIG. 9. Plot of the phonon momentum density P over T_m^3 (g cm^{-2} sec^{-1} °K^{-3}) as a function of the mean temperature T_m for different free-path ratios Λ for the parameters specified in Fig. 7. In the absence of impurities, we obtain the usual horizontal line P_0/T_m^3.

[13] W. J. de Haas and Th. Biermasz, Physica **2**, 673 (1935); **4**, 752 (1937).
[14] B. Berman *et al.*, Phys. Rev. **142**, 79 (1966).
[15] I. Pomeranchuk, J. Phys. (USSR) **6**, 237 (1942).

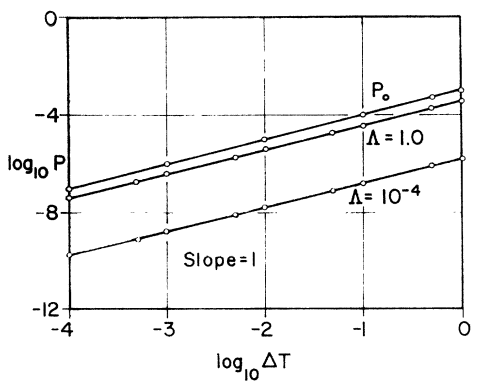

FIG. 10. Phonon momentum density P (g cm^{-2} sec^{-1}) as a function of the temperature difference ΔT(°K) across the slab for different free-path ratios Λ. The parameters of the log-log plot are the same as in Fig. 7.

Hence,

$$\kappa \propto a^{1/4} N^{-3/4}, \tag{8.9}$$

independent of T. The exact calculation gives these same dependencies. For other than Rayleigh scattering, i.e., for $\lambda_k \propto N^{-1} k^{-m}$ $(m \neq 4)$ the Pomeranchuk argument does not yield correct predictions: Here only the more exact theory provides the dependence on the impurity concentration N, temperature T, and slab thickness $2a$.

In contrast to its complicated dependence on the temperature, *the momentum density is a simple linear function of the temperature difference* ΔT between the slab boundaries for any value of the impurity concentration or free-path ratio. This may be seen in Fig. 10, where ΔT varies over four orders of magnitude, up to $\Delta T = T_m$. The heat flux is reduced by a factor of 2.7 for $\Lambda = 1$, and by a factor of 600 for $\Lambda = 10^{-4}$, at $T_m = 1$°K. "This linear dependence on ΔT does not hold true in the low impurity limit when the temperature difference ΔT becomes greater than the mean slab temperature T_m, i.e., $1 < \Delta T/T_m$ 2. In this region, therefore, the equation $Q = \kappa \Delta T/2a$ becomes invalid and is replaced by a new more complicated dependence of Q on ΔT [see Eq. (5.8)]."

The effect of the scatters may be viewed as producing a backflow, or reverse current of phonons, which for very high-impurity concentration finally cancels the forward current produced by the temperature difference. This viewpoint is illustrated in Fig. 11. Here, this reverse momentum density P_1 is plotted as a function of the central-slab temperature T_m. The free-path ratio is used as a parameter to obtain a set of curves. For large free path ratio the backflow is small, and is proportional to T_m^7, as may be seen from the analytical solution. As the free-path ratio decreases, the curves approach an asymptotic curve with T^3 dependence. The latter curve represents a backflow P_1 which is equal in magnitude but opposite in sign to the unobstructed flow P_0. The shaded region in Fig. 11 represents the area wherein all curves lie for $10^{-4} < \Lambda < 10^4$.

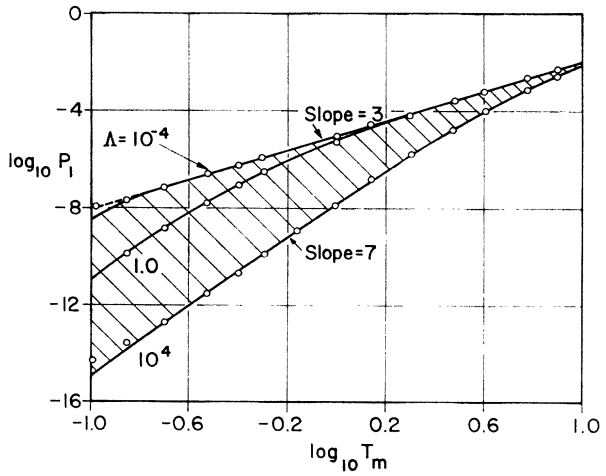

FIG. 11. Correction P_1 (g cm^{-2} sec^{-1}) to the momentum density due to scattering as a function of central slab temperature T_m(°K) for different free-path ratios Λ. All parameters are the same as in Fig. 7.

Spatial Distribution of Temperature

After this discussion of the momentum density or heat flux, let us summarize our results concerning the *energy density* $E(x)$. From the latter quantity we obtain the *local temperature* $T(x)$ through (5.16), the temperature being proportional to the fourth root of the energy density. Figure 12 shows the temperature as a function of position across the slab, for different free-path ratios Λ. Note, that for all four curves shown the temperature difference across the slab is the same: $\Delta T = 10$ mdeg.

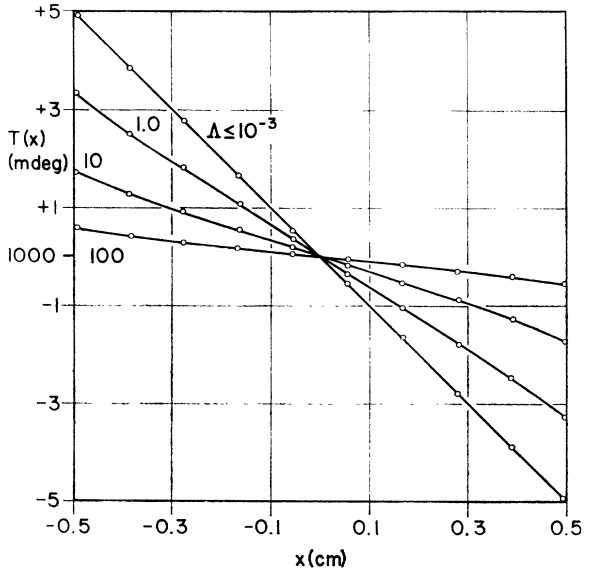

FIG. 12. Distribution of the temperature T as a function of position x across a slab of 1 cm thickness for different free-path ratios Λ, for phonons of velocity $c_s = 10^5$ cm sec^{-1}. The numerical results are obtained with a discretization parameter $n = 10$. For all four curves the temperature difference across the slab is $\Delta T = 10$ mdeg.

For a large free-path ratio $\Lambda > 100$, the temperature is practically constant across the slab and equal to T_m. The reason for this is that scattering is negligible and at all points in the slab a thermometer will receive the same flux of phonons originating at the two reservoirs. Hence, the temperature will everywhere inside the slab be the average of T_1 and T_2, and will discontinuously rise or drop to T_1 and T_2, respectively, at the slab boundaries.

As the free-path ratio decreases a temperature gradient develops in the slab: The discontinuity at the boundaries decreases, and disappears in the high-impurity-concentration limit. For $\Lambda < 10^{-3}$, the temperature is seen to decrease linearly from T_1 to T_2 across the slab, and the formula

$$T(x) = T_m - \tfrac{1}{2}\Delta T(x/a) \tag{8.10}$$

becomes valid.

In the region of intermediate-impurity concentration ($\Lambda = 1.0,\ 10,\ 100$) the numerical results show that the temperature distribution in the slab is still linear. It may be observed, that the calculated points at the boundaries do not fall on the straight lines which can be drawn through the other points. Therefore, the lines are drawn slightly bent at their ends. It is not possible to say, whether this bend is significant, or a result of numerical inaccuracy. The latter is more likely to be the case, because the distance over which the deviation from linearity occurs seems to have no relation to the only two physical parameters of the problem which have the dimension of a length: the slab thickness $2a$, and the free path λ.

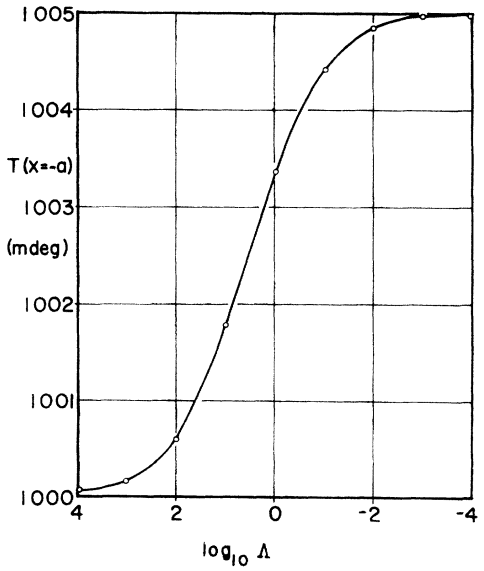

FIG. 13. Temperature drop at the interface of the heat reservoir and the conducting slab ($x = -a$), plotted as a function of the logarithm of the free-path ratio Λ. The central-slab temperature is $T_m = 1000$ m°K, that of the reservoir is $T_m + \Delta T/2 = 1005$ m°K, and the phonon velocity is $c_s = 10^5$ cm sec^{-1}.

Finally, Fig. 13 shows the variation of the temperature drop at the boundary as a function of the free-path ratio. This temperature drop, which may be termed the *Kapitza resistance* of the slab, varies from more than 99% of ΔT at $\Lambda \geqq 10^4$ to less than 1% of ΔT for $\Lambda \leq 10^{-3}$. This again indicates, that if a phonon is scattered more than 20 times on the average while crossing the slab, classical thermal conductivity theory becomes valid, and the Kapitza resistance is absent.

IX. REMARKS ON TRANSPORT COEFFICIENTS OF IMPERFECT CRYSTALS

In conclusion, we would like to add a few remarks concerning the implications of this work for the general theory of transport coefficients of solids. That is, we include in our consideration also such phenomena as the electrical conduction in disordered alloys, etc., and try to predict certain features of these phenomena from what we learned from the problem discussed in the preceding sections. At present, transport coefficients are most frequently calculated by means of linear response theory[16] or the *method of Green functions*[17] used in conjunction with some truncation procedure. These methods most often lead to *Kubo-type*[18] *formulas*. These formulas will certainly give *wrong answers*, if the generalized driving forces (temperature gradient, electric field) are large, or if the product of scattering cross section σ and concentration of scatterers N is large.

Let us first discuss *strong driving forces*. Two basic assumptions of linear response theory are violated in this case: The distribution function, hence the density matrix, is not close to the equilibrium function, and therefore cannot be written as the equilibrium function plus a small correction which is linear in the driving force. How much the phonon distribution function differs from equilibrium even for a small value of $\Delta T/T_m$ may be seen in Fig. 2. For $\Delta T/T_m \simeq 1$ our theory is still valid, but of course linear response theory becomes prohibitive.[19]

The other, related assumption found in the derivation of linear response theory is the validity of phenomenological equations which assume the *currents* to be *proportional to the driving forces*. We have seen, that due to the finite dimensions of our system such equations are not valid if the mean free path is not much smaller than the dimensions of the system. Hence, the driving forces cannot be considered to be *a priori* given. This can be seen in (5.8) where the heat flux depends (for fixed T_m) on ΔT and ΔT^3, as well as in Fig. 13, which shows a temperature drop at the boundaries, making the concept of a temperature gradient illusory in this case.

[16] J. M. Luttinger, Phys. Rev. **135**, A1505 (1964).
[17] D. N. Zubarev, Usp. Fiz. Nauk **71**, 71 (1960) [English transl.: Soviet Phys.—Usp. **3**, 320 (1960)].
[18] R. Kubo, J. Phys. Soc. Japan **12**, 570 (1957).
[19] For the case of electrical conductivity in strong fields, see W. A. Schlup, Physik Kondensierten Materie **7**, 124 (1968).

While it is generally recognized that linear response theory is restricted to the case of weak driving forces, the limitations of this and of the Green-function approach to small scattering strengths $N\sigma$ needs to be pointed out.

We have seen that *in the high-impurity-concentration limit the thermal conductivity became a nonanalytic function of* $N\sigma$ [namely, $\kappa \propto (N\sigma)^{-3/4}$]. Consequently, any theory which uses a *series expansion* in terms of integral powers of $N\sigma$ (even if it is a self-consistent theory) will certainly yield erroneous or *divergent results* for the system considered here. Similar occurences may not be excluded, for instance, in treating the conductivity of disordered alloys, where the concentrations of different constituents are of the same order of magnitude.

In the limit of low-impurity concentration, the formula developed in the text gives the result that the conductivity is reduced by an amount proportional to $N\sigma$ (5.10). If one carries the approximation one step further, one finds that the next correction is of the order $(N\sigma)^2(a+b\ln N\sigma)$. Hence even *in the low-impurity limit, a series-expansion-type solution is expected to diverge when carried beyond the first term* ($\ln N\sigma$ cannot be expanded.) Therefore, transport coefficients obtained by approximations—such as the truncation of chains of equations for Green functions—can only be trusted if the accuracy of the approximation can be estimated (or if the results agree with experiments.)

ACKNOWLEDGMENT

Our thanks are due to Edgar A. Rhodes for numerous helpful comments, particularly in connection with the computational problems.

APPENDIX A: CROSS SECTION AND FREE-PATH RATIO

Consider particles in a box of volume V in plane-wave states of the discrete spectrum. The wave function of each particle is given by

$$\psi(\mathbf{k}) = (1/V^{1/2})e^{i\mathbf{k}\cdot\mathbf{r}}. \tag{A1}$$

The particle density is $1/V$.

For elastic scattering, the probability $dW_{\mathbf{k}\mathbf{k}'}$ that particles in an initial state $\psi(\mathbf{k})$ make a transition to a final state $\psi(\mathbf{k}')$ per unit time is

$$dW_{\mathbf{k}\mathbf{k}'} = (2\pi/\hbar)|\mathcal{U}_{\mathbf{k}\mathbf{k}'}|^2\delta(\epsilon_k - \epsilon_{k'}), \tag{A2}$$

with $\mathcal{U}_{\mathbf{k}\mathbf{k}'}$ given in the Born approximation by

$$\mathcal{U}_{\mathbf{k}\mathbf{k}'} = \frac{1}{V}\int U(\mathbf{r})e^{i(\mathbf{k}-\mathbf{k}')\cdot\mathbf{r}}d^3r. \tag{A3}$$

$U(\mathbf{r})$ is the scattering potential of one scattering center.

Making use of the linear dispersion relation for phonons $\epsilon_k = c_s\hbar k$ and passing to the limit of a large box so that the transitions involve states in the continuum, (A2) becomes, summing over $\mathbf{k}'$ within an element of solid angle $d\Omega'$,

$$W_{\mathbf{k}d\Omega'} = \frac{Vd\Omega'}{(2\pi)^3}\int \frac{2\pi}{c_s\hbar^2}|\mathcal{U}_{\mathbf{k}\mathbf{k}'}|^2\delta(k-k')k'^2dk'. \tag{A4}$$

After integration,

$$W_{\mathbf{k}d\Omega'} = \frac{V}{(2\pi)^2}\frac{|\mathcal{U}_{\mathbf{k}\mathbf{k}'}|^2}{c_s\hbar^2}k^2d\Omega'\Big|_{k=k'} \tag{A5}$$

is the probability of transition of one phonon with wave vector $\mathbf{k}$ into a solid angle $d\Omega'$. Since the number of phonons incident on a unit area perpendicular to $\mathbf{k}$ is c_s/V, the quantity

$$d\mathcal{S}_k = \frac{W_{\mathbf{k}d\Omega'}}{c_s/V} = \left(\frac{V}{2\pi c_s\hbar}\right)^2|\mathcal{U}_{\mathbf{k}\mathbf{k}'}|^2k^2d\Omega'\Big|_{k=k'} \tag{A6}$$

represents the differential scattering cross section. The quantity $d\mathcal{S}_k$ is independent of the volume V because $|\mathcal{U}_{\mathbf{k}\mathbf{k}'}| \propto V^{-2}$.

Assuming isotropic scattering ($\mathcal{U}_{\mathbf{k}\mathbf{k}'} = \mathcal{U}_k$), the total cross section per unit volume for N scattering centers per unit volume is

$$\mathcal{S}_k = 4\pi\frac{d\mathcal{S}_k}{d\Omega'} = \frac{N}{\pi}\left(\frac{V}{c_s\hbar}\right)^2|\mathcal{U}_k|^2k^2, \tag{A7}$$

where $|\mathcal{U}_k|^2 \propto 1/V^2$.

In order to establish the correspondence between σ_0 defined in Ref. 5 and $\mathcal{S}_k$, note that $f_{\mathbf{k}}(x)$ is the number of phonons per unit volume with wave vector $\mathbf{k}$ at the point $\mathbf{x}$. The Boltzmann equation dictates that the collision operator $L_{\mathbf{k}}^{\text{imp}}\{f_{\mathbf{k}}(x)\}$ be the rate of change by scattering of $f_{\mathbf{k}}(x)$ per unit volume. Since $dW_{\mathbf{k}\mathbf{k}'}$ represents the transition probability for V^{-1} phonons per unit volume, we have, for N scattering centers per unit volume

$$L_{\mathbf{k}}^{\text{imp}}\{f_{\mathbf{k}}(x)\} = NV\sum_{\mathbf{k}'}[f_{\mathbf{k}}(x) - f_{\mathbf{k}'}(x)]dW_{\mathbf{k}\mathbf{k}'} \tag{A8}$$

for the continuous spectrum

$$\sum_{k'} \rightarrow \frac{V}{(2\pi)^3}\int d^3k',$$

and

$$L_{\mathbf{k}}^{\text{imp}}\{f_{\mathbf{k}}(x)\} = \frac{V}{(2\pi)^3}\frac{2\pi NV}{c_s\hbar^2}\int[f_{\mathbf{k}}(x) - f_{\mathbf{k}'}(x)] \times|\mathcal{U}_k|^2\delta(k-k')d^3k'. \tag{A9}$$

Now according to Ref. 5 the collision operator is

$$L_{\mathbf{k}}^{\text{imp}}\{f_{\mathbf{k}}(x)\} = \frac{V}{(2\pi)^3}\int[f_{\mathbf{k}}(x) - f_{\mathbf{k}'}(x)]\sigma_{\mathbf{k}\mathbf{k}'}d^3k' = \frac{V}{(2\pi)^3}\frac{2\pi N\sigma_0}{c_s\hbar^2}\int[f_{\mathbf{k}}(x) - f_{\mathbf{k}'}(x)] \times k^{m-2}\delta(k-k')d^3k'. \tag{A10}$$

(Note: m as defined here is $m+2$ of Ref. 5.) Comparison of (A9) and (A10) shows that

$$|\mathcal{V}_k|^2=\sigma_0 k^{m-2}/V\propto 1/V^2. \tag{A11}$$

By defining $\sigma=V\sigma_0$, substitution of (A11) in (A7) gives the desired relation

$$\mathcal{S}_k=N\sigma k^m/\pi c_s^2\hbar^2. \tag{A12}$$

Note, that by definition, σ is independent of the volume.

We define the phonon free path $\lambda_{\rm ph}(k)$ by

$$\lambda_{\rm ph}(k)\mathcal{S}_k=1, \tag{A13}$$

and the free-path ratio $\Lambda(k)$ by

$$\Lambda(k)=\lambda_{\rm ph}(k)/2a. \tag{A14}$$

The latter is a dimensionless parameter.

APPENDIX B: EVALUATION OF THE MOMENTUM INTEGRAL

In the high-impurity-scattering limit the momentum integral (5.5) is

$$P=2\pi\Omega\hbar\int_0^1\mu^2d\mu\int_0^\infty\frac{k^3C^0}{\xi k^m+\mu}dk. \tag{B1}$$

Making a change of variables in (B1) we set

$$z=\frac{c_s\hbar k}{k_BT_m}\quad\text{and}\quad\zeta=\xi\left(\frac{k_BT_m}{c_s\hbar}\right)^m, \tag{B2}$$

and for $\Delta T/T_m\ll 1$ use

$$C^0=\Delta T\frac{df^0}{dT_m}=\frac{\Delta T}{T_m}ze^z(f^0)^2. \tag{B3}$$

Thus, (B1) becomes

$$P=2\pi\Omega\hbar\left(\frac{k_BT_m}{c_s\hbar}\right)^4\frac{\Delta T}{T_m}\int_0^1\mu^2K(\mu)d\mu, \tag{B4}$$

where

$$K(\mu)=\int_0^\infty\frac{z^4e^z(f^0)^2}{\zeta z^m+\mu}dz. \tag{B5}$$

In order to evaluate $K(\mu)$ we write the argument as an exponential $e^{F(z)}$, where $F(z)$ is given by

$$F(z)=4\ln z+z+2\ln f^0-\ln(\zeta z^m+\mu). \tag{B6}$$

This function has a maximum at

$$z_0=\left(\frac{2\mu}{(m-2)\zeta}\right)^{1/m} \tag{B7}$$

under the assumption that $\zeta\gg 1$. It can be shown that for $l<z_0^{-1}$ the lth derivatives of $F(z)$ depend on z_0^{-l}, the maximum. We expand $F(z)$ into a Taylor series around z_0 and find

$$F(z)=F(z_0)+\sum_{l=2}^\infty a_l\left(\frac{z-z_0}{z_0}\right)^l, \tag{B8}$$

where

$$a_l=z_0{}^lF^{(l)}(z_0)/l! \tag{B9}$$

turns out to be independent of z_0. Substituting (B7) and (B8) into (B5) and changing variables yields

$$K(\mu)=\frac{m-2}{m}\left(\frac{2}{(m-2)\zeta}\right)^{3/m}\mu^{(3-m)/m}I \tag{B10}$$

with

$$I=\int_{-1}^\infty\exp\left(\sum_{l=2}^\infty a_lt^l\right)dt. \tag{B11}$$

Substituting (B10) into (B4) and integrating over μ gives the desired result (5.6). If the calculations above are carried out without assuming that $\Delta T/T_m\ll 1$, one obtains the same result (5.6) that the momentum density P is proportional to T_1-T_2.